
Article:
Vriend, N.M., McElwaine, J.N., Sovilla, B. et al. (3 more authors) (2013) High resolution radar measurements of snow avalanches. Geophysical Research Letters, 40 (4). pp. 727-731.

https://doi.org/10.1002/grl.50134

High-resolution radar measurements of snow avalanches

N. M. Vriend,[1] J. N. McElwaine,[1,2] B. Sovilla,[2] C. J. Keylock,[3] M. Ash,[4] and P. V. Brennan[4]

Received 3 October 2012; revised 19 December 2012; accepted 27 December 2012.

[1] Two snow avalanches that occurred in the winter 2010–2011 at Vallée de la Sionne, Switzerland, are studied using a new phased array FMCW radar system with unprecedented spatial resolution. The 5.3 GHz radar penetrates through the powder cloud and reflects off the underlying denser core. Data are recorded at 50 Hz and have a range resolution better than 1 m over the entire avalanche track. We are able to demonstrate good agreement between the radar results and existing measurement systems that record at particular points on the avalanche track. The radar data reveal a wealth of structure in the avalanche and allow the tracking of individual fronts and surges down the slope for the first time.
Citation: Vriend, N. M., J. N. McElwaine, B. Sovilla, C. J. Keylock, M. Ash, and P. V. Brennan (2013), High-resolution radar measurements of snow avalanches, *Geophys. Res. Lett.*, *40*, doi:10.1002/grl.50134.

1. Introduction

[2] Geophysical mass flows, such as snow avalanches, are a major hazard in mountainous areas and have a significant impact on the infrastructure, economy, and tourism of such regions. Obtaining a thorough understanding of the dynamics of snow avalanches is crucial for protecting infrastructure, and while hazard zoning and risk estimation may be based on the historical record of past events [*Keylock et al.*, 1999], detailed understanding of impact pressures can only come from accurate models [*Salm et al.*, 1990]. Models have been developed for many years, and with careful parameter choices, individual events can be replicated. However, because the underlying physics is poorly understood and measurements are difficult to make, significant uncertainties still remain.

[3] Direct observations of the denser core of a large avalanche are particularly difficult, since it is frequently obscured by the dilute powder cloud. Photogrammetry and videogrammetry may measure the dynamics of the outer edge of the powder cloud but cannot penetrate into the denser, more destructive core. For these reasons, there are no observations that accurately track the denser core of a large avalanche at high spatial and temporal resolution. Probes and sensors mounted in the avalanche path are successful in obtaining impact pressures, velocities, and flow depths as functions of time [*Sovilla et al.*, 2010] but are limited to only a few points on the track. Doppler radar measurements have been performed since the 1980's [*Gubler et al.*, 1986], and recent work has been focused at the large-scale test sites in Switzerland [*Rammer et al.*, 2007] and at Ryggfonn in Norway [*Gauer et al.*, 2007]. However, the range resolution of these instruments is limited to approximately 50 m, which is too coarse to resolve structures in the avalanche. Our radar has been installed at the Vallée de la Sionne avalanche test site in Switzerland (Figures 1a–1c) and has been collecting data since the 2010–2011 winter. In this paper, we present the first results from this system, which show a good agreement with other measurement systems.

2. The Radar System and Signal Processing

[4] We have developed an FMCW (Frequency Modulated Continuous Wave) phased array 5.3 GHz radar, whose technical specifications were described in *Ash et al.* [2010, 2011]. The system emits up and down chirps of different lengths, all with a bandwidth of 200 MHz, from a single transmitter. Eight receivers arranged in a sparse-sampled linear array (of ≈ 5 m base width) collect the reflected signal. Each channel is mixed with the outgoing chirp before being filtered and digitally sampled. Post-processing of the data from the eight receivers can aim the beam across the slope by, in effect, dividing the slope into strips with different lateral positions. However, in this paper, we average laterally across the slope. The radar wavelength is 57 mm; therefore, it mostly penetrates the dilute powder cloud with little attenuation. Reflections will mainly occur from the upper surface of the dense flowing layer and from blocks of snow within it [*Rammer et al.*, 2007]. Any blocks larger than the order of a wavelength will give significant reflections, so that discrete avalanche fronts will also be recorded by our radar. It is these discrete fronts that have proven easier to track and which we focus on in this paper. Reflections from both individual blocks and the surface of the dense layer make feature tracking within the core of the flow a difficult analysis problem. Radar of this wavelength can penetrate 10 m into dry snow and at least 2 m into solid ice [*Rignot et al.*, 2001], so there will also be reflections from layers in the underlying snow pack and from the ground. Thus, the amplitude of the reflected signal is a complicated function of both the snow avalanche and basal surface. The return data are averaged across all eight receivers and then Fourier transformed, giving a signal that describes the reflected intensity in time as a function of distance from the bunker. By subtracting

All Supporting Information may be found in the online version of this article.

[1]Department of Applied Mathematics and Theoretical Physics, University of Cambridge, Cambridge, UK.
[2]WSL Swiss Federal Institute for Snow and Avalanche Research, SLF, Davos, Switzerland.
[3]Department of Civil and Structural Engineering, University of Sheffield, Sheffield, UK.
[4]Department Electronic and Electrical Engineering, University College London, London, UK.

Corresponding author: N. M. Vriend, Department of Applied Mathematics and Theoretical Physics, University of Cambridge, Cambridge CB3 0WA, UK. (n.m.vriend@damtp.cam.ac.uk)

0094-8276/13/10.1002/grl.50134

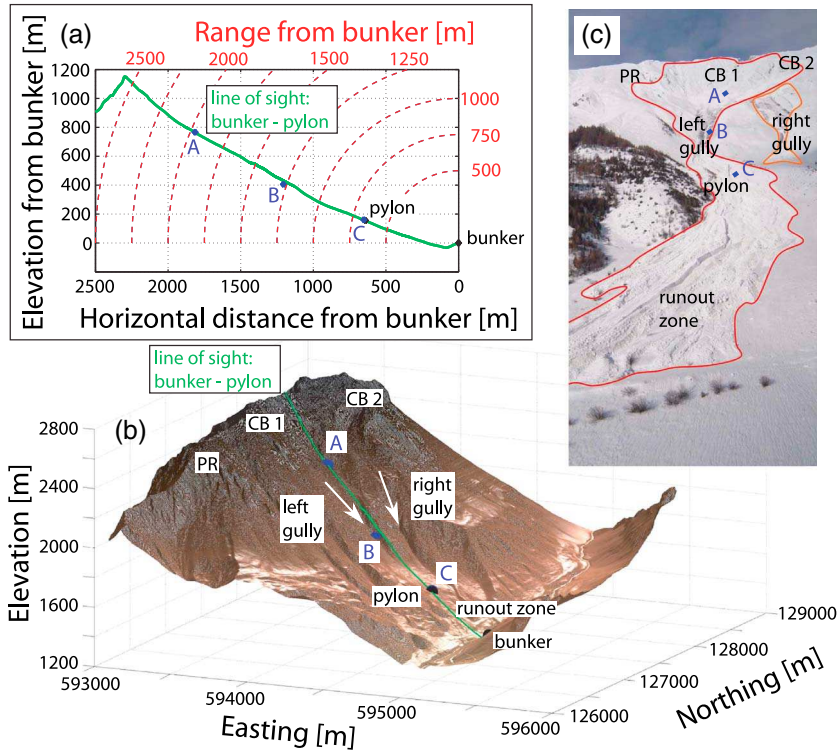

Figure 1. Overview of Vallée de la Sionne avalanche test site in Switzerland: (a) 2-D and (b) 3-D topographical rendering of the avalanche site with annotations; (c) photo of the avalanche debris in the morning of 7 December 2010.

the signal amplitudes from one chirp to the next, the background reflectivity is canceled. The resulting signal only contains information on moving targets, with intensity related to the depth-integrated mass flux. This procedure is known as Moving Target Identification (MTI), and a space-time plot is shown in Figure 2a. Where there is no moving snow, the plot is white or lightly colored. The transitions to a darker intensity show the arrival of avalanche fronts, and the change in position with time of these edges are the instantaneous avalanche front velocities. Inside the avalanche, the reflectivity constantly changes giving a medium intensity signal. Lines of maximum darkness correspond to surges or waves in the avalanche. Some of these are easily identified visually, but others are very hard to see and we find them using the Hough transform, an imaging processing technique for finding straight lines in images [*Duda and Hart*, 1972]. The transition from dark to white occurs again in the tail of the avalanche as it stops. This transition can have a finite gradient/velocity if the tail of the avalanche is moving, for example, behind front 1 in Figure 2c. If the avalanche simultaneously comes to a halt, the edge will be vertical, corresponding to an infinite phase velocity, which can be seen behind front 2 in Figure 2a. Because the plots are averaged across the slope, lines and edges can cross each since they correspond to features at different lateral locations (Figure 2d).

3. Setup of Field Experiments

[5] The Vallée de la Sionne avalanche test site in Switzerland [*Ammann*, 1999] is operated by the WSL Institute for Snow and Avalanche Research SLF and is located in the Swiss Alps near Anzère. Observations are primarily of naturally occurring avalanches, but when conditions are suitable, avalanches are triggered by explosives deployed by helicopter. The site features three main release zones—Pra Roua (PR), Crêta Besse 1 (CB 1), and Crêta Besse 2 (CB 2)—which lead into two gullies (left and right), and then a runout zone with a fairly uniform slope (Figures 1b and 1c).

[6] In the middle of the slope is a 20 m high pylon equipped with various sensors measuring flow velocity, depth and pressure [*Sovilla et al*., 2008; *Kern et al*., 2009]. Ground-based frequency modulated continuous wave (FMCW) radar [*Gubler et al*., 1986] has been buried in the ground at three locations: A, B, and C. A reinforced concrete bunker is situated on the opposite slope and houses researchers and equipment, including the phased array radar system. The eight receiver antennas are mounted on the outside wall of the bunker, and the radar is connected to the automatic seismic detection system located at A and B.

4. Natural Avalanches in December 2010

[7] We report on data from two naturally occurring dry snow avalanches from December 2010, denoted by SLF as #20103003 and #20103004. For more details, see *Kogelnig et al*. [2011] and the Supporting Information.

4.1. #20103003

[8] Event #20103003 occurred at 18:31 on 6 December 2010. The initial release and acceleration were not observed as the seismic trigger had a significant delay (Figure 2a). The leading front at zero time is positioned well beyond the release zone at a range of 1200 m and has a constant velocity front.

[9] The avalanche originated from CB 1 and/or PR and did not pass over the FMCW radar at A. The main flow

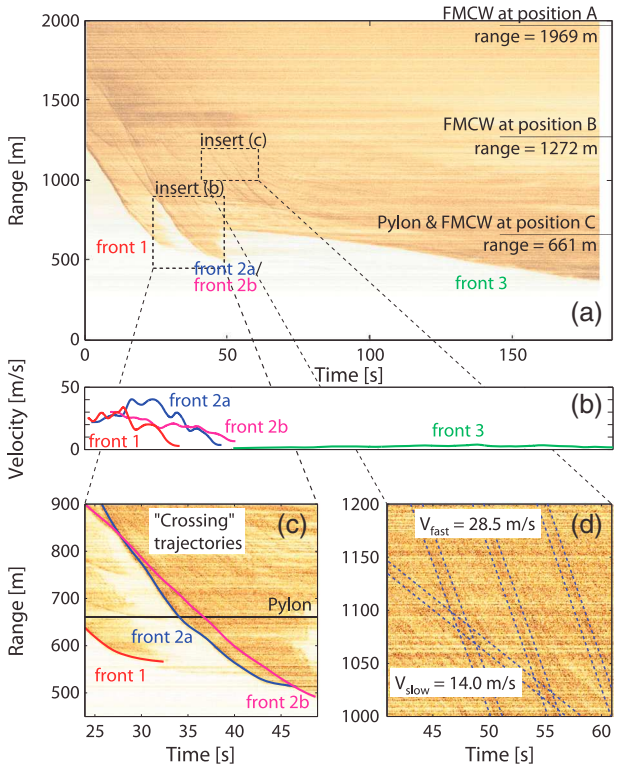

Figure 2. Moving target indication (MTI) of the radar measurement of avalanche #20103003 on 6 December 2010 at 18:36. Dark colors represent changes in radar reflectivity due to movement of the snow, plotted against time and distance from the bunker. (a) Three individual avalanche fronts move downhill at different times over the 3 minute recording interval. (b) Higher up the slope, there are two crossing fronts, Figures 2a and 2b. These are probably different avalanches separated laterally. (c) Flow features in the body of the avalanche—two different velocities $V_{fast} = 28.5$ m/s, with fronts spaced 5 s apart, and $V_{slow} = 14.0$ m/s are present (identified using the Hough transform).

followed the left gully, passed over the FMCW radars at B and C and beside the pylon. Figures 2a and 2b show that the avalanche develops three distinct fronts, the second of which may be divided into separate trajectories (Figure 2c). The first two travel at a maximum velocity of 30 and 40 m/s, respectively, move past the pylon and position C to a range of approximately 500–550 m, and stop abruptly. Above 1100 m, the snow pack was cold and dry, but below this altitude, it was wetter and much warmer, so there was no longer any dry snow to entrain and the drag increased. The third front is a slowly moving (1–3 m/s) dense avalanche, readily distinguished based on the amplitude of its reflectivity, which is still mobile when the recording finishes after 3 min. This front has either entrained moist snow or the remnants of the avalanche, from which the more dynamic fronts have separated. Such uniform, slow avalanches have been previously observed and discussed in *Sovilla et al.* [2010].

4.2. #20103004

[10] Avalanche #20103004 occurred at 03:36 on 7 December 2010 and started from CB 1 and/or CB 2. Front 1 of the avalanche moved down the left-hand gully, over the FMCW radars at B and C and past the pylon. Panels (c) and (d) in the photographical account in the Supporting Information show that the avalanche dug a trough through the earlier deposits, finally coming to rest further down the slope. A second front came down the right-hand gully and ran over the deposit from a previous avalanche.

[11] The MTI plot (Figure 3) shows several different moving targets in the release zone (1500–2500 m), corresponding to horizontally separated avalanches, which then combine at around 1400 m. Figures 3b and 3c illustrate the evolution of the velocity of avalanche front 1 as a function of range and time, respectively. The main front traveled very fast (40 m/s) in the upper part of the mountain but started to decelerate rapidly from a range of 1100 m, finally moving slowly at 5–10 m/s in the run-out area at a range of 320 m, where the data acquisition ended. This deceleration is also due to the change in snow pack as discussed earlier.

[12] A secondary front, visible deeper in the recording and marked as front 2, travels at a lower velocity (12 m/s, decelerating to a few meters per second) and a larger range (1400 m, closing to 900 m), as illustrated in Figures 3d and 3e. The right-hand gully opens up around 1100 m, where the velocity in Figure 3d drops significantly. Based on evidence from the depositional features and information obtained from the ground-based radar data, we conclude that the second front moved into the right-hand gully and diverted its path from the main front.

5. Cross-Comparison of Our Instrument With Existing Data

[13] The goal of the current study is to compare the new phased array radar measurements with existing velocity data of the optoelectronic sensors [*Tiefenbacher and Kern*, 2004] at the pylon, and the time evolution of snow cover at positions A and B measured with the ground-based FMCW radars [*Gubler et al.*, 1986].

[14] Figure 4 shows a comparison between the phased array radar and the ground-based FMCW radar. Event #20103003 did not pass over FMCW A, as no avalanche tail exists in the FMCW recording. The leading edge of the avalanche had already passed FMCW B when the recording started in Figure 4a, but the internal fronts of the phased array radar match up well with the peaks in the ground-based FMCW radar. The comparison for event #20103004 at position A in Figure 4b is very strong—the individual streaks in the phased array radar match very closely the FMCW radar. The agreement is less apparent for position B in Figure 4c, as there is a lack of identifiable features in both recordings. Interestingly, the second arrow belonging to front 2 does not correlate with the data from the FMCW radar at position B. We believe that this disagreement is because the internal front follows the right-hand gully, which has not been instrumented with ground-based FMCW radar.

[15] Figure 5 compares the velocity data obtained from the optoelectronic sensors on the pylon with the velocity deduced from the phased array radar for events #20103003 and #20103004.

[16] Figure 5a shows the velocities for avalanche #20103003 at different heights on the pylon as a function of time. The three front structures, two fast and dilute and one slow and dense, are clearly visible, and the arrival times match up perfectly with the MTI plot 5b. Figures 5a$_1$ and 5a$_2$

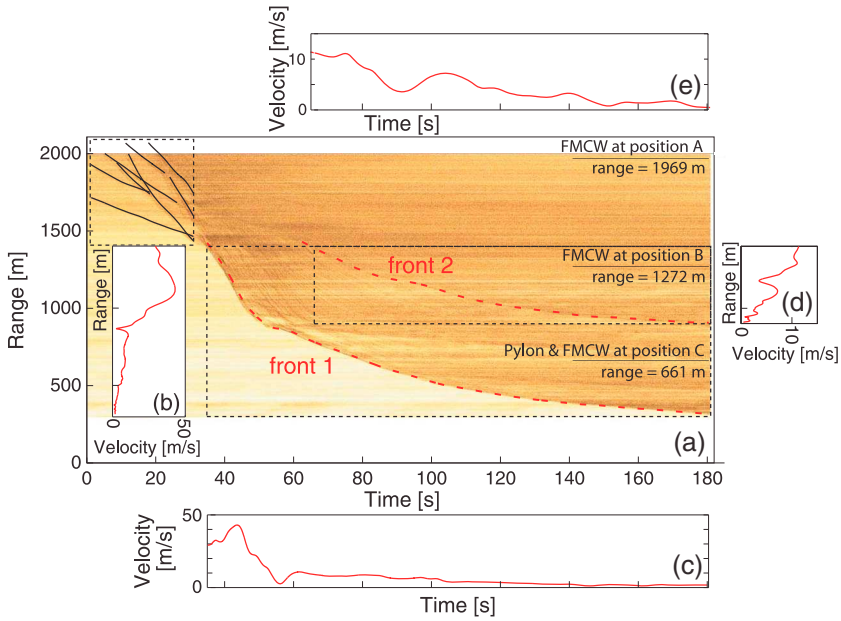

Figure 3. Moving target indication (MTI) of the radar measurement of avalanche #20103004 on 7 December 2010 at 03:36. (a) Front 1 moves downhill over the whole 3 min recording interval; front 2 moves down the right hand gully later in time. The velocity of front 1 has been illustrated in (b) as a function of range and in (c) as a function of time; the velocity of front 2 has been plotted in (d) as a function of range, and in (e) as a function of time with matching axis to the main plot.

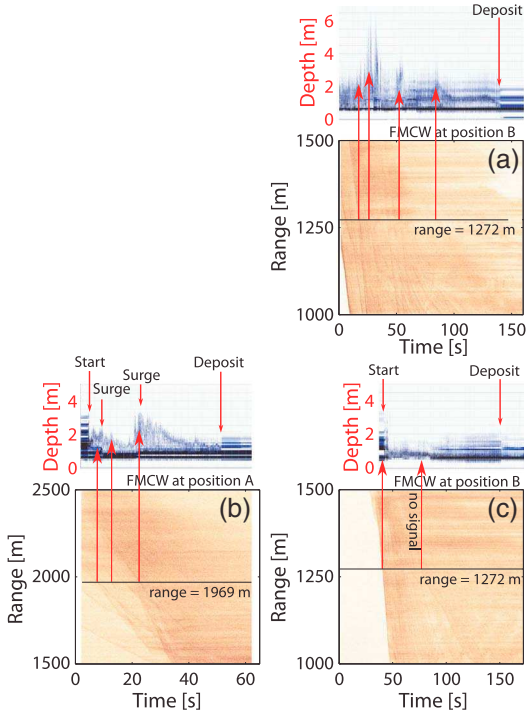

Figure 4. Comparison between the phased array radar data and the FMCW radar data: (a) at position B for #20103003, (b) at position A for #20103004, and (c) at position B for #20103004. Note that the FMCW radar is a point measurement, while the phased array radar measures the whole of the front; thus, unless the tip of the front passes directly over the FMCW position, the phased array radar will show an earlier arrival.

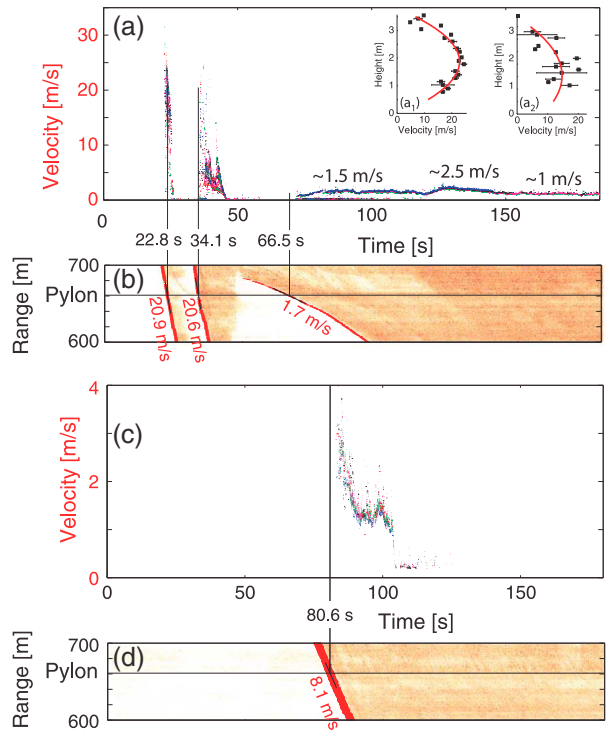

Figure 5. Comparison between (a) the optoelectronic velocity sensor data and (b) the radar data at the pylon for #20103003. The insets (a_1) and (a_2) show the vertical velocity profiles for the first two fronts. The data for #20103004 are shown in (c) and (d). Each color in the optoelectronic data represents the data from a sensor at a different height—they are spaced every 125 mm.

show the velocity profiles for the first two fronts at their greatest depth. The peak velocities in these profiles are a little larger than the MTI-calculated velocity. For the third front, the velocity of the optoelectronic sensors shows an almost constant reading with depth and agrees closely to the velocity obtained from the radar (1.5 and 1.7 m/s, respectively), but the timing of the radar arrival is slightly earlier than the arrival registered by the optoelectronic sensors. Front 3 appears to be a dense, plug-like granular flow.

[17] Figures 5c and d illustrate the comparison for event #20103004—the signal of the radar is both early and arrives at a much higher velocity than the optoelectronic sensor reading (8.1 versus 1–3 m/s), suggesting that the front of the avalanche passed to the side of the pylon.

6. Conclusion and Future Work

[18] This study presents a new state-of-the-art high-resolution phased array radar system that is able to image snow avalanches along the entire avalanche track. The radar data have been compared successfully to the timing and velocity of the fronts recorded by other sensors located at discrete positions in the avalanche track. The velocity evolution of the entire front as a function of time and range shows a correlation between snow-pack properties and topographic features, and accelerations and decelerations. It was previously difficult to infer such relations with older instruments with a 50 m spatial resolution. A key component of avalanche models is the dependence of basal friction on avalanche speed and depth. By being able to follow flow features over the whole track, we expect our data to be of major importance in validating existing theories and developing improved avalanche models. For example, the resolution of our data permits, for the first time, the time derivative of the temporal velocity profile to be determined with high accuracy, yielding a data-derived estimate of the relevant structure and coefficients of a flow friction law [Ancey and Meunier, 2004].

[19] This system has the potential to track avalanches simultaneously over the entire slope with high spatial and temporal resolution. Future work will include the calibration of all eight radar channels to permit beam forming, thus resolving the avalanche across the slope. By the correct processing of up and down chirps, it is also possible to measure the velocity directly by Doppler methods, rather than feature tracking as performed in this paper. This will require the development of new signal processing techniques, as existing methods are designed for discrete targets rather than continuous sources.

[20] **Acknowledgments.** The authors would like to thank the technical staff as well as François Dufour of the Swiss Federal Institute of Snow and Avalanche Research and Martin Kern for their help throughout the duration of this work. The authors also thank the Natural Environment Research Council for their support, grant reference NE/F004621/1.

References

Ammann, W. J. (1999), A new Swiss test site for avalanche experiments in the Vallée de la Sionne/Valais. *Cold Reg. Sci. Tech.*, *30*, 3–11.

Ancey, C., and M. Meunier (2004), Estimating bulk rheological properties of flowing snow avalanches from field data, *J. Geophys. Res.*, *109*, F01,004, doi:10.1029/2003JF000036.

Ash, M., K. Chetty, P. Brennan, J. McElwaine, and C. Keylock (2010), FMCW radar imaging of avalanche-like snow movements, in Radar Conference, 2010 IEEE, pp. 102 –107, doi:10.1109/RADAR.2010.5494643.

Ash, M., P. V. Brennan, N. M. Vriend, J. N. McElwaine, and C. J. Keylock (2011), FMCW phased array radar for automatically triggered measurements of snow avalanches, in Proceedings of the 8th European Radar Conference, pp. 166–169, EuMA.

Duda, R. O., and P. E. Hart (1972), Use of the Hough transformation to detect lines and curves in pictures. *Comm. ACM*, *15*, 11–15.

Gauer, P., M. Kern, K. Kristensen, K. Lied, L. Rammer, and H. Schreiber (2007), On pulsed Doppler radar measurements of avalanches and their implication to avalanche dynamics, *Cold. Reg. Sci. Tech.*, *50*, 55–71.

Gubler, H., M. Hiller, G. Klausegger, and U. Suter (1986), Messungen an Fliesslawinen. Zwischenbericht 1986, Eidg. Inst. für Schnee- und Lawinenforsch., Weissfluhjoch, Switzerland, *41*.

Kern, M. A., P. Bartelt, B. Sovilla, and O. Buser (2009), Measured shear rates in large dry and wet snow avalanches, *J. Glaciol.*, *55*(190), 327–338.

Keylock, C. J., D. M. McClung, and M. Magnusson (1999), Avalanche risk mapping by simulation, *J. Glaciol.*, *45*, 303–314.

Kogelnig, A., E. Suriñach, I. Vilajosana, J. Hübl, B. Sovilla, M. Hiller, and F. Dufour (2011), On the complementariness of infrasound and seismic sensors for monitoring snow avalanches, *Nat. Hazards Earth Syst. Sci.*, *11*, 2355–2370, doi:10.5194/nhess-11-2355-2011.

Rammer, L., M. Kern, U. Gruber, and F. Tiefenbacher (2007), Comparison of avalanche-velocity measurements by means of pulsed Doppler radar, continuous wave radar and optical methods. *Cold. Reg. Sci. Tech.*, *50*, 35–54.

Rignot, E., K. Echelmeyer, and W. Krabill (2001), Penetration depth of interferometric synthetic-aperture radar signals in snow and ice, *Geophys. Res. Lett.*, *28*(18), 3501–3504, doi:10.1029/2000GL012484.

Salm, B., A. Burkard, and H. Gubler (1990), Berechnung von Fliesslawinen. Eine Anleitung für Praktiker mit Beispielen, *Mitt. Eidg. Institut Schnee-und Lawinenforschung*, 47.

Sovilla, B., M. Schaer, M. Kern, and P. Bartelt (2008), Impact pressures and flow regimes in dense snow avalanches observed at the Vallée de la Sionne test site, *J. Geophys. Res.*, *113*, F01,010, doi:10.1029/2006JF000688.

Sovilla, B., J. N. McElwaine, M. Schaer, and J. Vallet (2010), Variation of deposition depth with slope angle in snow avalanches: Measurements from Vallée de la Sionne, *J. Geophys. Res.*, *115*, F02,016, doi:10.1029/2009JF001390.

Tiefenbacher, F., and M. A. Kern (2004), Experimental devices to determine snow avalanche basal friction and velocity profiles. *Cold. Reg. Sci. Tech.*, *38*, 17–30.